Merged-beams measurements of electron-capture cross sections for $O^{5+}+H$ at electron-volt energies

C. C. Havener, M. S. Huq, H. F. Krause, P. A. Schulz,* and R. A. Phaneuf
Oak Ridge National Laboratory, Oak Ridge, Tennessee 37831-6372
(Received 17 August 1988)

Absolute total cross-section measurements are presented for electron capture in $O^{5+}+H(D)$ collisions over the energy range 0.9–800 eV/amu. These are the first experimental data to be reported using a new multicharged-ion–atom merged-beams apparatus developed at Oak Ridge National Laboratory. The experimental method and the cross-section measurements are described in detail. At energies below 2 eV/amu, the data show a cross-section enhancement which may be attributed to the ion-induced dipole attraction between the reactants. Agreement with recent unpublished quantum-mechanical calculations ranges from fair at the lower energies to excellent at the higher energies.

I. INTRODUCTION

The inelastic process whereby a multicharged ion captures an electron from a neutral atom is important in environments containing both highly charged ions and neutral atoms. Cross sections for this electron-capture process at low energies are typically large ($>10^{-15}$ cm^2) and selectively populate excited states of the multiply charged ion. Such collisions, therefore, are important for plasmas of thermonuclear fusion, astrophysics, multicharged ion sources, and the development of x-ray lasers.

In such low-velocity collisions ($v<1$ a.u.), the relative nuclear motion between collision partners is slow compared to the orbital motion of the active electrons in the system. Electrons of the temporary quasimolecule formed in the collision have sufficient time to adjust to the changing interatomic field as the nuclei approach and separate. As one proceeds to lower energies, any attempt to theoretically predict cross sections must treat the complex electronic structure of this quasimolecule. For velocities in the range $0.1<v<1$ a.u. the behavior of the total capture cross section has been successfully parametrized in terms of ionic charge, target binding energy, and collision velocity. A discussion of various theoretical models which have been applied to collisions of atoms with highly charged ions may be found in the monograph by Janev *et al.*[1] A short description of different experimental approaches and scaling methods for collisions of multicharged ions with atomic hydrogen may be found in the review of Gilbody.[2] With the development of advanced sources of multiply charged ions, such as the electron-cyclotron-resonance (ECR) ion source, sufficient beam intensities have become available to systematically study electron capture for bare ions[3] and to determine the cross section for population of different final (excited) states in beam-gas measurements. Both translational-energy[4] and optical spectroscopy[5] have proven successful in providing experimental tests for theory in this energy range.

For still lower velocities ($v<0.1$ a.u.) less is known about electron capture by multicharged ions colliding with neutral atoms. Most of the theoretical development has focused on simple one-electron systems, such as fully stripped ions colliding with atomic hydrogen. Coupled stationary-state calculations,[6,7] while successful at higher energies, do not necessarily give consistent predictions at lower energies. In such calculations, the internuclear motion has generally been treated classically. Full quantal calculations may be required for accurate predictions at the lowest energies, but such methods have remained essentially untested.[8] At these low energies near or below 1 eV/amu there has been speculation that orbiting may occur.[8–10] According to this simple classical model,[11] as the ion and neutral atom approach each other, the ion induces a dipole on the neutral atom, causing an attraction which may lead to orbiting trajectories. For sufficiently low velocities these orbits decay until at some critical internuclear distance charge transfer may take place. Cross sections due to this process are predicted to have a $1/v$ dependence at lower energies. Although actual "orbiting" may not occur in such collisions, trajectory effects due to this attraction may enhance the electron transfer cross section.

Most of the experimental work on such collision processes has been based on ion-beam gas-target methods, which have been generally limited to energies above 100 eV/amu. Some experiments at lower energies have been performed by Phaneuf *et al.*[12] using a pulsed-laser–produced plasma as a source of slow multiply charged ions. In the 10–100-eV/amu energy regime they found that for few-electron systems there exists no simple scaling with charge or velocity, so that each system must be investigated separately. To address this subject in more detail, an ion-atom merged-beams apparatus has been developed at Oak Ridge National Laboratory (ORNL) to measure absolute total electron-capture cross sections for multicharged ions colliding with atomic hydrogen in the energy range of 1–1000 eV/amu.

The merged-beams method is well suited for such measurements in this low-energy range.[13] In this technique keV beams of neutral atoms and multicharged ions are merged such that the relative velocity of the two beams corresponds to the desired collision energy. Absolute cross sections are obtained from measurement of all experimental parameters. The identical relative velocity may be created in many different ways: by appropriately scaling the laboratory energies of the multicharged ion and neutral beams, by interchanging the faster and slower species, or by isotopic substitution. These different laboratory kinematic conditions provide important diagnostic and stringent consistency checks on the method. Due to the simple kinematics of the transformation from the laboratory to the center-of-mass frame, any uncertainty in the energy of the neutral or ion beam is deamplified in the moving center-of-mass frame. Likewise, large angular scattering[14] of the reaction products in the moving center-of-mass frame is compressed when transformed to the laboratory frame.

The purpose of this paper is to present the results of the first absolute merged-beams measurements of electron-capture cross sections for the collision system

$$O^{5+}+H \rightarrow O^{4+}+H^{+}$$

in the relative energy range of 0.9–800 eV/amu. Included is a discussion of the merged-beams technique along with a detailed description of the experimental apparatus used to perform the measurements.

II. MERGED-BEAMS TECHNIQUE

The concept of using merged beams to measure interactions at low relative energies has been discussed in the literature.[13] Although these experiments are technically difficult, there have been several successful experiments involving atomic or molecular species in ion-ion,[15,16] ion-neutral,[13,17–21] and neutral-neutral[22] collisions in which reactions have been studied from thermal to several hundred eV in energy. However, these experiments have involved only singly or doubly charged ions heretofore.

When two beams intersect, their relative interaction energy is given by

$$W=\frac{\mu}{2}|\mathbf{V}_1-\mathbf{V}_2|^2 , \tag{1}$$

where μ is the reduced mass $m_1 m_2/(m_1+m_2)$, and $m_i, \mathbf{v}_i$ the mass and initial velocity of each projectile. Dividing by μ and writing Eq. (1) in terms of the energy of each beam, E_i, and the intersection angle θ between the two beams, the relative energy in the center-of-mass frame becomes

$$E_{\rm rel}=W/\mu=\frac{E_1}{m_1}+\frac{E_2}{m_2}-2\left[\frac{E_1}{m_1}\frac{E_2}{m_2}\right]^{1/2}\cos\theta . \tag{2}$$

For perfectly collinear beams, $\theta=0$ and $E_{\rm rel}$ can be made zero for $E_1/m_1=E_2/m_2$.

Figure 1 is a simplified schematic of the apparatus which illustrates the merged-beams technique. The O^{5+} beam from the ORNL-ECR ion source is merged electrostatically with a neutral H or D beam. The merged beams interact in a field-free region for a distance of 80.8 cm, after which the primary beams are magnetically separated from each other and from the product or "signal" H^+ ions. The O^{4+} product of the reaction is not measured separately but is collected together with the primary O^{5+} beam in a large Faraday cup. The neutral-beam intensity is measured by secondary-electron emission from a stainless-steel plate, and the signal H^+ or D^+ ions are recorded by a channel electron multiplier (CEM) operated in the pulse-counting mode.

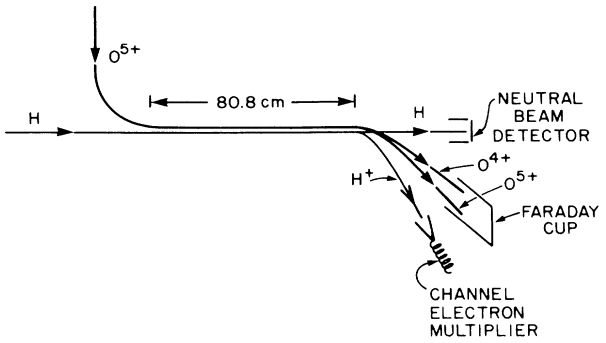

FIG. 1. Simplified schematic of the ion-neutral merged-beams apparatus, using the $O^{5+}+H$ system as an example.

Figure 2 shows the relative energy in the center-of-mass frame, $E_{\rm rel}$, obtained for three different neutral-

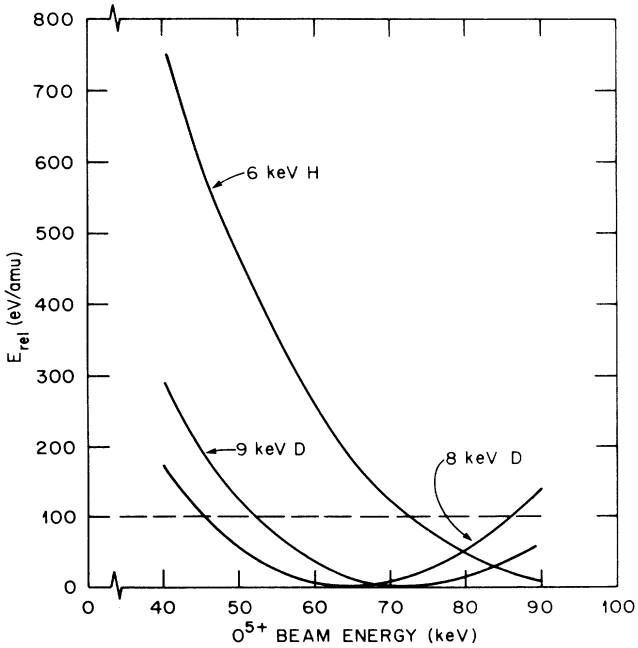

FIG. 2. Relative energy $E_{\rm rel}$ obtainable in the present apparatus for 6-keV H, 8-keV D, and 9-keV D neutral beams as a function of the O^{5+} beam energy. The intersections of the horizontal line at 100 eV/amu with the different H (D) curves illustrate that several different laboratory conditions can be used to measure the cross section at a given $E_{\rm rel}$.

beam conditions. To change the energy E_{rel}, the energy of the O^{5+} is varied while the velocity of the H or D beam is held constant. It is clear from the figure that a wide range of relative energies ($\sim 0.1-800$ eV/amu) is obtainable with this apparatus for this collision system. For an 8-keV D beam, velocity matching occurs with an O^{5+} beam energy of 64 keV. Therefore, for an O^{5+} beam energy <64 keV, the D travels faster than the O^{5+}, and for an energy >64 keV, the D travels slower than the O^{5+}. When other H- and D-beam energies are considered, one value of E_{rel} may be obtained under several different laboratory conditions. For example, as seen in Fig. 2, an interaction energy of 100 eV/amu may be obtained in several ways: D faster, D slower, and H faster than the O^{5+} beam. These different laboratory conditions provide important diagnostic checks on the measurements.

An important advantage of the merged-beams technique is the large deamplification of the interaction-energy uncertainty resulting from energy uncertainties in the primary beams. This deamplification effect can be seen in Fig. 2. The slope of the curves is just $\Delta E_{rel}/\Delta E_2$, where ΔE_2 is the energy uncertainty in the O^{5+} beam. As E_{rel} decreases, the slope decreases, reducing the uncertainty in E_{rel}. For an estimated uncertainty of 10 eV in the neutral-beam energy and 100 eV in the O^{5+}-beam energy, the estimated uncertainty in the collision energy due to each beam is less than 1 eV/amu at $E_{rel}=100$ eV/amu and 0.1 eV/amu at $E_{rel}=1.0$ eV/amu. The lowest relative energy obtainable with the apparatus is not limited by the uncertainty in the beam energies, but rather by imperfect collimation and alignment of the beams (see Sec. IV).

Perhaps the most important advantage of the merged-beams technique in low-energy measurements is the potentially large angular collection of the reaction products. The low-energy electron-capture collisions under study are exoergic, and, since both products are positively charged, they can involve significant angular scattering[14] in the center-of-mass frame. Therefore, experiments must be designed with as large an angular collection of products as possible. In this respect the merged-beams technique is ideal since the angular scattering in the center-of-mass frame becomes significantly compressed in the laboratory frame, the frame in which the product ions are collected. This angular compression can be evaluated by examining the kinematic transformation in more detail.

After the collision the exoergicity of the reaction, Q, is added to the relative energy of the colliding particles. Hence, the final energy in the center-of-mass frame is

$$T_r^f=\tfrac{1}{2}\mu v_r^{f\,2}=\tfrac{1}{2}\mu v_r^{i\,2}+Q \ . \tag{3}$$

This additional energy is shared between the two product ions in accordance with the conservation of linear momentum. Let us assume for simplicity that the lighter projectile m_1 is traveling faster than m_2; then after the collision the final velocities v_1^f and v_2^f are given by

$$v_1^f=V_{c.m.}+\frac{\mu}{m_1}v_r^f \ , \tag{4a}$$

$$v_2^f=V_{c.m.}-\frac{\mu}{m_2}v_r^f \ . \tag{4b}$$

The faster of the two collision partners gains in velocity, while the slower loses. Figure 3 shows the vector (Newton) diagram for this collision with the angle $\theta_{c.m.}$ and θ_{lab} shown for the lighter projectile m_1. It is evident that the larger the center-of-mass velocity $V_{c.m.}$, the greater the angular compression in the laboratory frame. The laboratory scattering angle θ_{lab} is related to the angle of scattering in the center of mass $\theta_{c.m.}$ by

$$\tan\theta_{lab}=\frac{(\mu/m_1)v_r^f\sin\theta_{c.m.}}{V_{c.m.}+(\mu/m_1)v_r^f\cos\theta_{c.m.}} \ . \tag{5}$$

Using Eq. (5) and an estimate of 1.8° for the angular collection in the laboratory (see Sec. III), the angular collection in the center-of-mass frame was calculated as a function of energy for several different neutral beams. As may be seen in Fig. 4, for measurements performed at an E_{rel} around 1 eV/amu with a 6-keV H neutral beam, up to 58° scattering of the signal (H^+ products) can be collected. By performing measurements at higher $V_{c.m.}$ and with D instead of H, the effective angular collection of the products in the center-of-mass frame can be significantly increased, providing an important diagnostic and indicating the extent of large angular scattering. For measurements performed at these low energies with a 9-keV D beam, all of the scattering in the center-of-mass frame can be collected in the laboratory.

Another aspect of the merged-beams technique is that the exoergicity Q of the reaction is amplified when transformed from the center-of-mass to the laboratory frame. For O^{5+} on H (D) at these low energies, capture takes place predominantly into the $n=4$ shell of O^{4+}.[23] If one assumes a statistical population of the $n=4$ sublevels, one can calculate an average energy for the final state. The difference in energy between the initial and final state of the transferred electron results in an exoergicity Q of 8.2 eV. Figure 5 shows the maximum shift in energy for an 8-keV D beam as a function of E_{rel}, due to the 8.2-eV

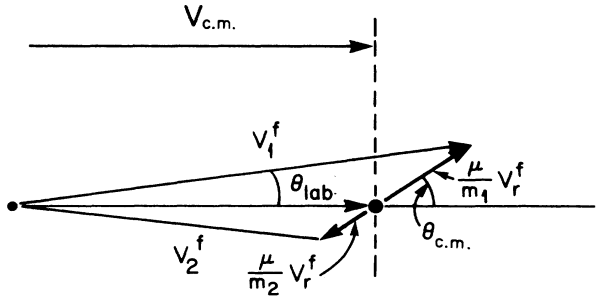

FIG. 3. Vector (Newton) diagram after the collision. The symbols v_1^f and v_2^f correspond to the final velocities of the projectiles with masses m_1 and m_2, respectively, in the laboratory frame. v_r^f is their final relative velocity.

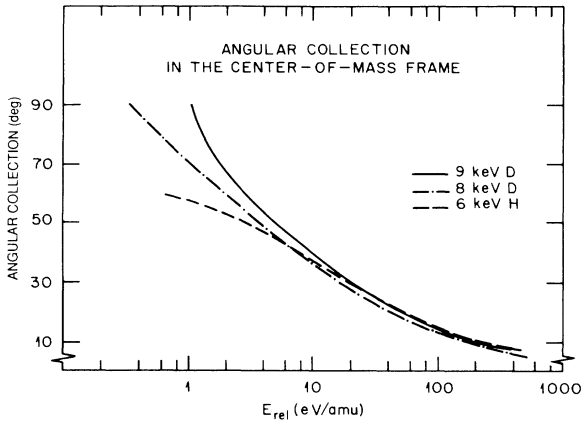

FIG. 4. Estimated angular collection of the reaction products in the center-of-mass frame as a function of E_{rel} for measurements performed with a 6-keV H, 8-keV D, and a 9-keV D neutral beam.

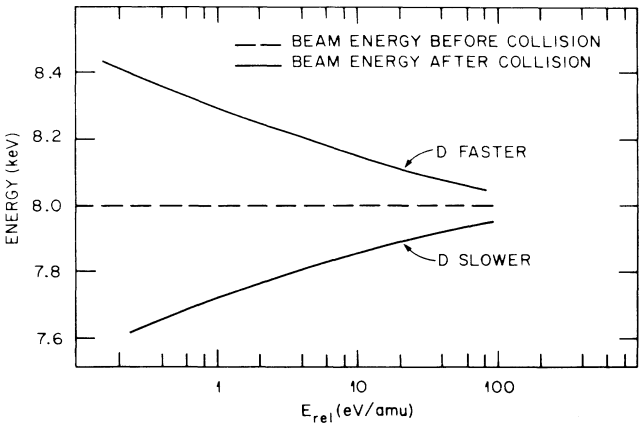

FIG. 5. Resultant energy in the laboratory frame of an initial 8-keV D beam after interaction with O^{5+}. 8.2 eV was used as the exoergicity Q of the reaction.

exoergicity. The maximum shift is calculated using Eq. (4) and assuming that scattering is restricted to the forward angle ($\theta=0$) for D faster than O^{5+} (upper curve) and to the backward angle ($\theta=180°$) for D slower (lower curve). Especially at low relative energies, these shifts can be large and, if experimentally observed, could be correlated to energy shifts in the center-of-mass frame, supplying information about the collision dynamics.[17,20,24] In some merged-beams experiments these shifts have been used to discriminate against background events.[16] This discrimination was not possible here because the apparatus was designed to provide a low-resolution energy dispersion of the products H^+ (D^+) (see Secs. III and IV).

Cross-section measurement

Electron-capture cross sections are determined by measuring the rate of H^+ (D^+) product ions produced by the beam-beam interaction over the merged length L. The cross-section value is calculated at each velocity from the directly measurable quantities through the equation

$$\sigma=\frac{R}{\epsilon}\frac{\gamma q e^2}{I_1 I_2}\frac{v_1 v_2}{v_r}\frac{1}{L\langle F\rangle}\ , \tag{6}$$

where R, I_1, and I_2 correspond to the measured-signal count rate, effective current produced by neutral particles, and O^{5+} current, respectively. The true signal rate is given by R/ϵ, ϵ being the efficiency of the CEM for detecting H^+ (D^+) at velocity v_1, and the true neutral "current" is I_1/γ, γ being the measured effective secondary-electron emission coefficient for the neutral-particle detector. The quantity q is the charge state of the ion, for O^{5+}, $q=5$, and e is the electronic charge. v_r is the relative velocity of the two beams. $\langle F\rangle$ is the effective form factor and is a measure of the spatial overlap of the two beams along the merged path L. Rigorously, $\langle F\rangle$ should be determined by integrating the product of the number densities n_1 and n_2 of the two beams at every point along the merged path. Properly normalized, $\langle F\rangle$ is then

$$\langle F\rangle=\frac{\int\int\int n_1(x,y,z)n_2(x,y,z)dx\,dy\,dz}{\int\int\int n_1(x,y,z)dx\,dy\,dz\int\int\int n_2(x,y,z)dx\,dy\,dz}\ , \tag{7}$$

where z is the direction of propagation of the beams and xy defines a plane perpendicular to the beams. Obviously some approximation must be made in order to make the measurement of $\langle F\rangle$ experimentally tractable.

The beam-beam overlap is measured at four different locations z_j along the merged path. At each of these positions, the beam-profile monitors perform two orthogonal one-dimensional scans of each beam, I_i, giving, in the notation of Eq. (7), at $z=z_j$,

$$I_i(y)=\int n_i(x,y,z=z_j)dx\ , \tag{8a}$$

$$I_i(x)=\int n_i(x,y,z=z_j)dy\ . \tag{8b}$$

Assuming that the numerator of Eq. (7) is separable in x and y and substituting what is actually measured [as shown in Eqs. (8a) and (8b)] Eq. (7) becomes

$$F(z=z_j)=\frac{\int I_1(y)I_2(y)dy\int I_1(x)I_2(x)dx}{\int I_1(y)dy\int I_1(x)dx\int I_2(y)dy\int I_2(x)dx}\ . \tag{9}$$

The integrals in the denominator are just the total integrated beam currents. By extrapolating and interpolating values for $F(z)$ along the merged path, an averaged value of F can be calculated.

Table I shows typical operating parameters at an interaction energy of 25 eV/amu. The true D^+ beam-beam signal rate R is 110 Hz and must be detected in the presence of a background of 6.24 kHz. Note that, according to Eq. (6), for the same cross section, the signal count rate is proportional to v_r and thus decreases as measurements are performed at lower E_{rel}. To determine R, a two-beam modulation scheme was used,[25] since both beams can contribute to the background count rate. The largest portion of the background comes from the neutral beam stripping collisions on background gas over the 80-cm merge path. Therefore, vacuum in the beam line was critical and had to be maintained as low as possible, typically around 2×10^{-10} Torr under experimental conditions. Further experimental details are presented in Sec. III.

III. EXPERIMENTAL PROCEDURE

A. Primary-beam production

A ground-state neutral H (D) beam is produced by photodetachment of a 10–20-μA beam of H^- (D^-) in a 150 W cw Nd:YAG laser cavity ($\lambda=1.06$) μm) (see Fig. 6). For our application, photodetachment has several advantages over the more common technique of using a charge exchange or detachment gas cell to produce a neutral beam. These advantages, as described by Van Zyl *et al.*,[26] include compatibility with ultrahigh vacuum, generation of a ground-state beam, and the ability to perform an *in situ* absolute calibration of the neutral-beam detector.

The 6–9-keV H^- (D^-) beam was produced by a commercial duoplasmatron ion source with an offset extraction anode for negative-ion production. A combination of a Pierce extractor, a cylindrical Einzel lens, and steering plates focus the beam on an aperture in front of a 30° bending magnet. This aperture serves to limit gas loading from the source (the pressure in the beam line before the magnet is typically 3×10^{-6} Torr) and as an object for a second Einzel lens located 65 cm downstream. The second lens, along with another set of steering plates, refocuses and positions the H^- (D^-) beam to overlap with the laser beam in the cavity where up to 0.5 kW of power circulates within a beam 1.6 mm in diameter. The laser cavity was extended to intersect the trajectory of the H^- beam by the use of an antireflection coated vacuum window and an externally adjustable water-cooled copper laser mirror *in vacuo*. Conversion of 0.5–1.0% of H^- (D^-) to H (D) produces a 2–4-mm full width at half maximum (FWHM) 10–20-particle nA H (D) beam in the merged path. The divergence of this beam is typically less than 0.2°. The unconverted H^- (D^-) beam is removed by a 90° parallel-plate electrostatic deflector. Steering and focusing elements before and after the deflector ensure 100% transmission of the H^- (D^-) beam to the beam dump. The beam dump is differentially pumped with a 1000-l/s titanium sublimator.

Two apertures, one just after the 30° bending magnet and one just before the location where the laser neutralization takes place, define a differentially pumped section to prevent gas loading in the merge chamber from the H^- (D^-) source. Vacuum in this section was maintained at 1.0×10^{-9} Torr by a 360-l/s turbomolecular pump, a 30-l/s ion pump, and a 1000-l/s titanium sublimator pump. Gas loading in the UHV merge chamber due to the H^- (D^-) and H (D) beams is less than 2.0×10^{-10} Torr. After the laser neutralization point there are no apertures that limit the H^- (D^-) or H (D) beams until they reach their detectors.

Because the H^- beam directly up- and downstream of the laser neutralization point has the proper trajectory, some reactant neutral atoms ($<1\%$) were produced by stripping on background gas rather than by the laser. Of these, there exists a small fraction ($<1\%$) of excited states.[27] These excited states can be photoionized by the laser, stripped by the electric field in the electrostatic deflectors, or survive and interact with the multicharged ion-beam producing beam-beam signal. This resulted in an estimated uncertainty in the cross section of a few percent (see Sec. IV).

The O^{5+} beam is provided by the ORNL-ECR ion source.[28] This source is well suited to the merged-beams experiment since the source along with its beam optics is able to produce multicharged ion beams which are stable in intensity, profile, and trajectory for many hours. The correct mass-to-charge ratio is selected by a 90° magnetic analyzer and the resultant beam is focused onto an aperture in front of the UHV merge chamber by a quadrupole lens and steering plates. This aperture, shown in Fig. 6, serves as an object for a combination of Einzel lenses and steerers which direct the multicharged ion beam through a second 90° electrostatic parallel-plate deflector and produce a 6–8-mm (FWHM) O^{5+} beam in the merged path with a mean divergence of less than 0.5°.

TABLE I. Typical operating parameters.

$O^{5+}+D\rightarrow O^{4+}+D^+$, $E_{rel}=25$ eV/amu	
Primary beams	
D: 8 keV, 8.5 nA (equivalent), $\gamma=1.10$	
O^{5+}: 54.33 keV, 1.9 μA	
Signal	110 Hz
Background	6.24 kHz
Signal-to-noise ratio:	1.76×10^{-2}
v_1v_2/v_r	1.024×10^{9} cm/sec
$\langle F\rangle$	2.35 cm^{-2}
σ_{54}	81×10^{-16} cm^2
Time for 10% standard deviation	3.6 min
Vacuum	
Merge chamber: 8×10^{-10} Torr	
Merge section: $1-2\times10^{-10}$ Torr	
Demerge chamber: 4×10^{-10} Torr	

B. Merge section

The effective merge path begins when the beams exit the 90° deflector (parallel-plate analyzers, see Fig. 6). A differential pumping aperture 12.7 mm in diameter is

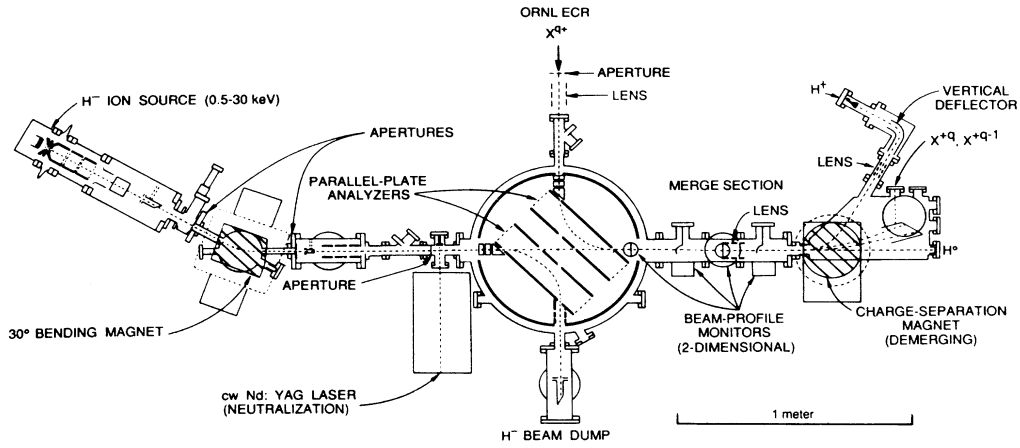

FIG. 6. Schematic of the ion-atom merged-beams apparatus.

placed near the beginning of the merge path and allows the pressure in the merged path to be maintained near 1×10^{-10} Torr, while the pressure in the merge chamber is 8×10^{-10} Torr with beams. This aperture does not limit the beams. The merge chamber is pumped with a 2000-l/s helium cryopump and a 1000-l/s titanium sublimator pump; the merge path by a 270-l/s ion and a 1000-l/s titanium sublimator pump. The H and O^{5+} beams interact along a 80.8-cm merge path and then are magnetically separated (see Fig. 6). UHV conditions must be maintained in the merge path to minimize background due to stripping of the H (D) beam as it travels through the background gas. Fortunately, the cross section for stripping on background gas ($\sim10^{-16}$ cm^2) at keV energies is much smaller than the cross section for electron capture collisions with O^{5+} ($\sim10^{-14}$ cm^2) at electron-volt energies. Nevertheless, in ultrahigh vacuum, the 80.8-cm merge path in residual gas constitutes a target on the order of 1000 times thicker than the O^{5+} beam traveling at nearly the same velocity as the H (D) beam.

C. Beam-beam overlap measurement

In order to determine the beam-beam overlap along the merged path, beam profiles are measured by four beam scanners at positions indicated in Figs. 6 and 7. The first and third-profile monitors are mechanical knife-edge scanners schematically shown in the Fig. 7(a). Since the knife edges are oriented $\pm45°$ to the vertical, the scanners measure horizontal (H') and vertical (V') profiles in a frame rotated 45° with respect to the single translation axis of the beam probe. As the probe is translated by ΔZ steps into and through the beams, transmission of the O^{5+} and H (D) beams is measured as a function of the position of the probe. Taking a derivative with respect to the distance translated in the rotated frame, $\Delta Z' = \Delta Z/\sqrt{2}$, gives the H' and V' profiles shown in Fig. 7(a). Profiles were obtained under computer control with

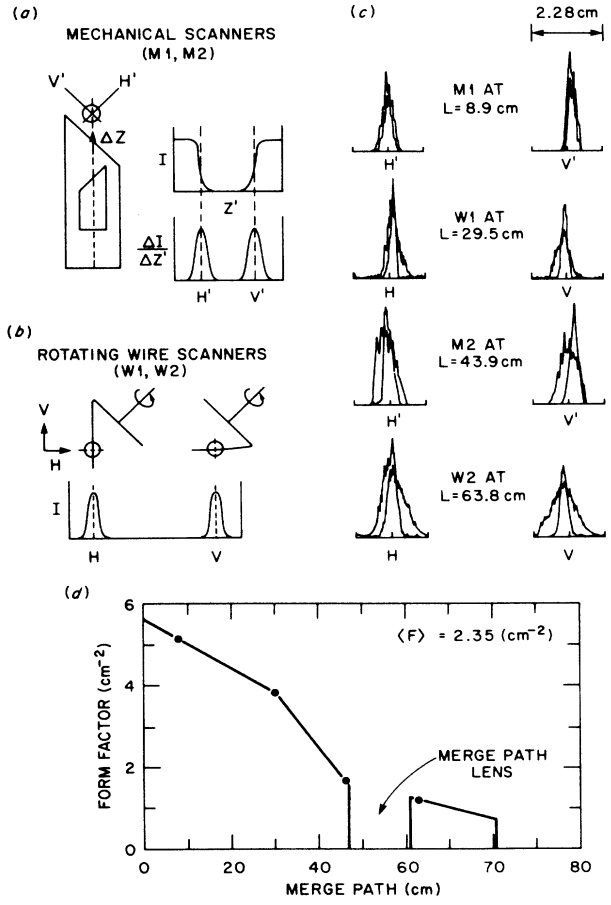

FIG. 7. (a) and (b) schematically show the operation of the mechanical knife-edge and rotating-wire scanners. (c) shows two-dimensional beam profiles at four locations along the merge path. (d) shows the four form factors F, calculated from the beam profiles along with interpolation-extrapolation as a function of position in the merge path.

the translation of the probe and measurement of the transmitted beams fully automated. An advantage of these knife-edge scanners is that the profiles of both beams are measured simultaneously. The H' and V' profiles each consists of 50 points scanning a distance of 1.12 cm, each point separated by 0.022 cm. These profiles can be used in Eq. (9) to give a form-factor measurement at two different positions along the merged path, approximating the integrals by finite sums. It should be noted that the knife-edge technique relies on measuring small differences in larger beam currents and is sensitive to fluctuations in the beam intensity. For subsequent measurements on other systems (e.g., N^{5+}), where the beam intensities are not sufficiently stable, the first knife-edge scanner M1 [see Fig. 7(c)] was replaced by a corresponding slit geometry.

The remaining two beam scanners in the merge path are commercial rotating-wire beam-profile monitors, schematically shown in Fig. 7(b). The principle of operation is as follows: A helical shaped 0.25-mm wire is rotated at 19 Hz in the beam in such a way that the beam "sees" a wire scanning horizontally and then vertically for a distance of ± 1.0 cm from the center of the scanner. An analog signal produced from the secondary electrons ejected from the wire is in direct proportion to the horizontal and vertical profiles of the beam [see Fig. 7(b)]. Properly synchronized with the rotation of the wire, the profiles of each beam can be displayed in real time on an oscilloscope. This facilitated tuning beams with minimum divergence and maximum overlap. The beam profiles are measured by recording these signals using a wave-form digitizer. Each profile consists of 201 points scanning 2.28 cm, the distance between points being 0.113 mm. The form factor is then determined using a finite-sum approximation to Eq. (9).

Figure 7(c) shows the beam profiles taken at the four positions along the merge path for the O^{5+} and D beams presented in Table I. At each position there are horizontal and vertical profiles of the ion and neutral beams, the latter being the narrowest, with a FWHM of 2 to 3 mm. The O^{5+} beam is generally larger, with a FWHM of about 6 to 8 mm, making the overlap of the two beams more stable. The first and third profiles, labeled M_1 and M_2, are taken with respect to a 45° rotated frame of reference, thereby indicating the elliptical nature of the beams, if any. Figure 7(d) shows the values of the four form factors calculated from the measured profiles plotted as a function of position along the merged path. Values for the remainder of the merge path are estimated by linear interpolation or extrapolation as shown in the figure. An Einzel lens is located 51 cm into the merged path to aid in collection of the products. Any products created inside the lens will be born at a different potential and will not be transmitted through the magnetic and electrostatic dispersion elements (see Fig. 6) to the detector. To account for this a zero form factor is assigned to the appropriate path length inside the lens. Beyond the lens angular collection of the signal is reduced, and it is estimated that only 50% of the signal from this region is collected. To account for this loss, F is assigned a value of half that shown in the figure in the region after the lens. Uncertainties due to this correction procedure are typically 6% or less. For the typical case presented in Fig. 7, the average $\langle F \rangle$ was calculated to be 2.35 cm^{-2}.

D. Demerge section

The function of the demerge section is to collect and monitor the two primary beams and to measure the product signal. Vacuum in this section is maintained at $\approx 4\times 10^{-10}$ Torr (with beams) by a 300-l/s ion and a 1000-l/s titanium sublimator pump. The H^+ (D^+) signal is magnetically deflected in the horizontal plane through 62.5° and then enters an Einzel lens and a 90° cylindrical analyzer where it is deflected out of the horizontal plane and focused onto the detector. The vertical deflection reduced by two orders of magnitude the photon background produced when the O^{5+} ions strike the surfaces in the Faraday cup. Large photon backgrounds have been observed in our laboratory to be characteristic of multicharged ions incident on surfaces. The same particle flux of H^+ or H^- ions on the same cup produced more than two orders of magnitude less background. The H^+ (D^+) detector is a 2.5-cm-diam. channel electron multiplier with an extended cone. Some early measurements using a 6-keV H beam were performed with a smaller CEM that had a 1-cm-diam. cone. In both cases the CEM cones and a 0.97% transmitting grid mounted directly in front were operated at a potential of -2.6 kV. Accelerating the H^+ (D^+) to -2.6 keV before striking the cone ensures 100% detection efficiency of the multiplier and rejects any stray secondary electrons. The grid also ensures that there are no nonuniform potentials across the aperture of the device which would degrade detector efficiency as a function of position on the cone.

The primary O^{5+} beam is measured in a Faraday cup biased to +90 V to ensure negligible loss of secondary electrons. Since the H^+ (D^+) signal is mechanically restricted to a horizontal deflection of 62.5° by the demerging magnet, the O^{5+} beam is deflected through a range of angles depending on the selected relative velocity of the two beams. To accommodate these different angles, the cup is mounted on a linear motion feedthrough that enables collection of any O^{5+} beam trajectory with a deflection angle in the magnetic field ranging from 15° to 55°.

The primary neutral H (D) beam is measured using secondary-electron emission from a 2.5-cm-diam. stainless-steel disk (see inset of Fig. 8). A guard ring based at +200 V draws electrons from the disc. The ratio of electrons emitted to neutral H or D striking the disc is γ, the secondary emission coefficient. The effective neutral current I_1 then, is given by I_{H_m}/γ, where I_{H_m} is the measured electron current leaving the disc. A procedure[26] for *in situ* absolute calibration of the neutral detector is as follows: The H^- (or D^-) beam intensity is measured in the beam dump with the laser alternately switched on and off. The intensity difference, ΔI_{H^-}, corresponds to the number of neutral H produced, and this difference is compared to the electron current leaving the disk, I_{Hm}. After several trials to average over

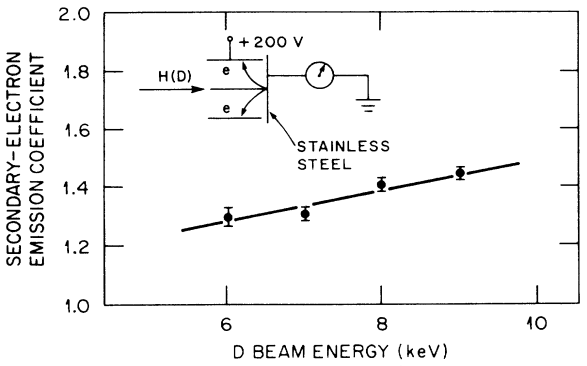

FIG. 8. Measurements of γ, the secondary emission coefficient for the neutral beam detector, are shown as a function of D-beam energy in keV. The inset is a schematic of the detector.

beam intensity fluctuations, the ratio $\gamma = I_{Hm}/\Delta I_{H^-}$ could be determined to within a reproducibility of 5%. Since the procedure relies on 100% transmission of both H^- and H to their detectors, great care had to be taken in tuning the beams accordingly.

After several measurements it was found that γ was stable for several weeks if the apparatus remained under vacuum. Typically, γ was measured to be in the range 1.1 ± 0.2, sometimes increasing 5–10 % after venting the apparatus to atmosphere with dry N_2. A slight incident-beam energy dependence was found and is shown in Fig. 8 for the various D-beam energies used. Experimental determination of γ to a few percent took several hours, thus determination of γ for every cross-section measurement was impractical. Often γ was measured at one energy, and then as the energy of the neutral beam was changed, the value of γ was scaled according to the measured energy dependence shown in the figure. It was, however, necessary to remeasure γ at some energy each time the system was opened to atmospheric pressure, and periodically to establish the stability over time.

E. Beam-modulation scheme

Table I shows typical operating parameters showing the various backgrounds encountered in the measurements. The case presented is for $E_{rel} = 25$ eV/amu with an 8.0-keV D and 54.3-keV O^{5+} beam. Most of the 6.24-kHz background arises from the 8.5-nA D beam stripping on background gas. Photons created by the 1.9-μA O^{5+} hitting the Faraday cup account for about 900 Hz of the background. Under these conditions, and for an average form factor, $\langle F \rangle$ of 2.35 cm^{-2}, the signal was measured to be 110 Hz. The cross section is calculated to be 81×10^{-16} cm^2. The ratio of signal to noise is measured to be 1.8×10^{-2} and the data-collection time required to obtain a signal with a 10% standard deviation of the mean was 3.6 min. Since the signal rate R scales with $\sqrt{E_{rel}}$ [see Eq. (6)], and the measured cross section is 68×10^{-16} cm^2 at $E_{rel} = 0.9$ eV/amu, the signal-to-noise ratio at this energy is decreased to 2.8×10^{-3}. For $E_{rel} = 766$ eV/amu, $\sigma = 37 \times 10^{-16}$ cm^2 and the signal-to-noise ratio increased to 4×10^{-2}.

To separate the signal from background, a two-beam modulation technique[25] was used. Both beams were switched on and off by applying 100–200 V between two parallel deflecting plates placed near where the ion beams were extracted from their respective sources. The logic for the beam switching and signal collection, as shown in Fig. 9, is computer generated and sent from a computer-aided measurement and control register to a fast voltage amplifier with a rise time of 0.5 μsec. During one complete cycle, scaler 1 records the H^+ (or D^+) signal counts due to beam-beam interaction along with the backgrounds generated by each beam. Scaler 2 records the background due to the O^{5+} and H beams separately. Both scalars 1 and 2 also measure any dark counts of the channel electron multiplier. Written out in terms of rates, the contents of scalers 1 and 2 after one complete cycle of period Γ are

$$N_{sc1} = \frac{\Gamma}{4}(R_{sig} + R_{H\,bg} + R_{O^{5+}\,bg}) + \frac{\Gamma}{2} R_{dark} , \quad (10a)$$

$$N_{sc2} = \frac{\Gamma}{4}(R_{H\,bg} + R_{O^{5+}\,bg}) + \frac{\Gamma}{2} R_{dark} . \quad (10b)$$

Subtracting the contents of scaler 2 from scaler 1 gives the signal. As shown in Fig. 9, there are delays of 22 μsec built into the logic [for simplicity these delays are not included in Eqs. (10)] to allow ample time for the beams to switch on or off, to stabilize, and to allow particle flight times from the switching plates to the merging region and detector. This results in a measured duty factor of 0.79 for a chopping period Γ of 500 μsec. This chopping scheme also incorporates other refinements to account for any small differences in scaler gating characteristics and also nonuniformities of beam intensities during the chopping period and is capable of separating a

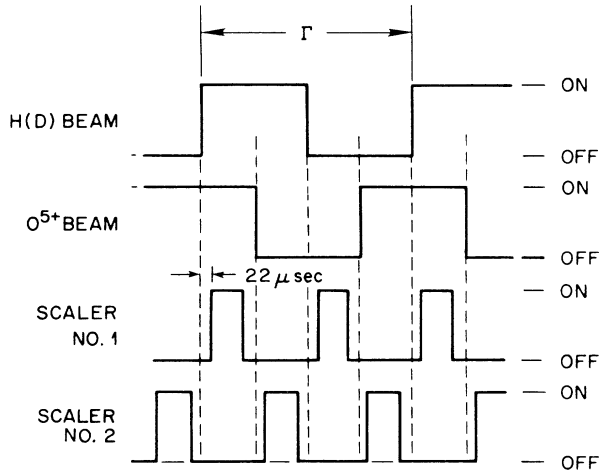

FIG. 9. Beam modulation scheme showing logic supplied by computer. Delays of 22 μsec are used to allow for beam settling. Γ denotes one complete period.

signal from background nearly 10^5 larger. Various possible spurious signals inherent in a chopping scheme have been discussed elsewhere.[25,29] Those encountered in this application are discussed in Sec. IV.

F. Signal collection

In order to perform measurements at low energies, the signal detector and beam optics must have as large an angular acceptance as is practical to collect all the H^+ (D^+) products of the beam-beam interaction along the merged path. To ensure large angular collection, a cylindrical Einzel lens was placed toward the end of the merged path. Trajectories of H^+ (or D^+) at several positions in the merge path were calculated using the SLAC electron trajectory code.[30] A few of these trajectories are shown in Fig. 10. It was found that trajectories originating in front of the merge-path Einzel lens with laboratory scattering angles of up to 2.5° from the beam axis are focused onto the detector. Angular collection after the lens is reduced and consequently all the products formed in this region with $> 1.1°$ of scatter in the laboratory are not collected. An effective maximum angular collection for the entire apparatus of 1.8° is calculated by weighting the maximum angular collection at each position by a typical beam-overlap factor [see Fig. 7(d)] F at that position and averaging over the merge path L.

The maximum angular collection in the laboratory ($\theta_{\text{lab}}^{\text{max}}$) corresponds to a much larger angular collection in the center of mass frame ($\theta_{\text{c.m.}}^{\text{max}}$) due to the kinematic transformation as discussed in Sec. II. The angular collection of a 9-keV D beam is considered consistent with all the data being reported here and values of $\theta_{\text{c.m.}}^{\text{max}}$ for different energies are shown in Table II. Note that at relative collision energies around 1 eV/amu, the angular compression ($\theta_{\text{c.m.}}^{\text{max}}/\theta_{\text{lab}}^{\text{max}}$) is as large as 50.

TABLE II. $\theta_{\text{c.m.}}^{\text{max}}$ and $\theta_{\text{lab}}^{\text{max}}$ for 9-keV $D+O^{5+}$

E_{rel} (eV/amu)	$\theta_{\text{c.m.}}^{\text{max}}$ (deg)	$\theta_{\text{lab}}^{\text{max}}$ (deg)	$\theta_{\text{c.m.}}^{\text{max}}/\theta_{\text{lab}}^{\text{max}}$
500	6	1.8	3.3
100	13	1.8	7.2
50	19	1.8	11
10	38	1.8	21
5	49	1.8	27
1	90	1.8	50

IV. SYSTEMATICS AND UNCERTAINTIES

A. Systematics

Figure 11 shows various diagnostic scans on the measured signal. The horizontal scan [see Fig. 11(a)] is accomplished by varying the demerging magnetic field which horizontally scans the signal and background across the signal Einzel lens, vertical deflector, and detector combination (see Fig. 6). The plateau on the background is approximately 25 G wide which corresponds to an energy width of 340 eV. As is observed in Fig. 11(a), the beam-beam signal is shifted in energy relative to the beam-gas background by ~ 10 G which corresponds to a 140-eV shift. This shift can be qualitatively understood as due to the kinematic amplification of the exoergicity of the reaction (see Sec. II). For the condition where the H beam is faster than the O^{5+}, it was observed, as it should be, that the H^+ signal shifted to higher energies relative to the background.

The low-energy resolution of the demerging magnet coupled with the large detector is an advantage, as it allows all the signal and background to be placed simultaneously on the detector. This was not found to be the case for some initial measurements performed with the smaller CEM. The plateaus of the signal and background were not as wide, and at energies near $E_{\text{rel}} = 25$ eV/amu both the signal and background could not be placed simultaneously on the detector. Attempts to measure a signal of a few hertz out of the kilohertz background positioned on the edge of the detector often led to spurious signals due to space-charge modulation of the trajectory of the H^+ beam by the O^{5+} beam. This space-charge modulation caused the background count rate to be different by a small amount when the O^{5+} beam was

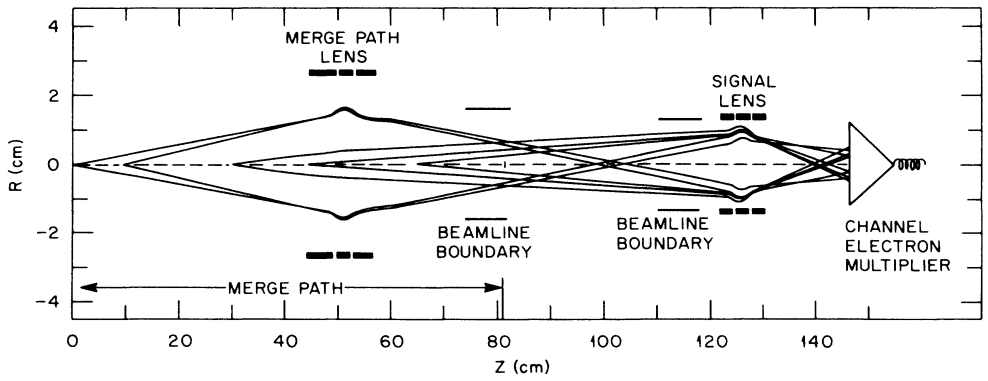

FIG. 10. Calculated trajectories for the H^+ (D^+) signal ions produced along the merge path and transmitted to the detector. The focusing properties of the demerging magnet and vertical deflector are negligible and are not included.

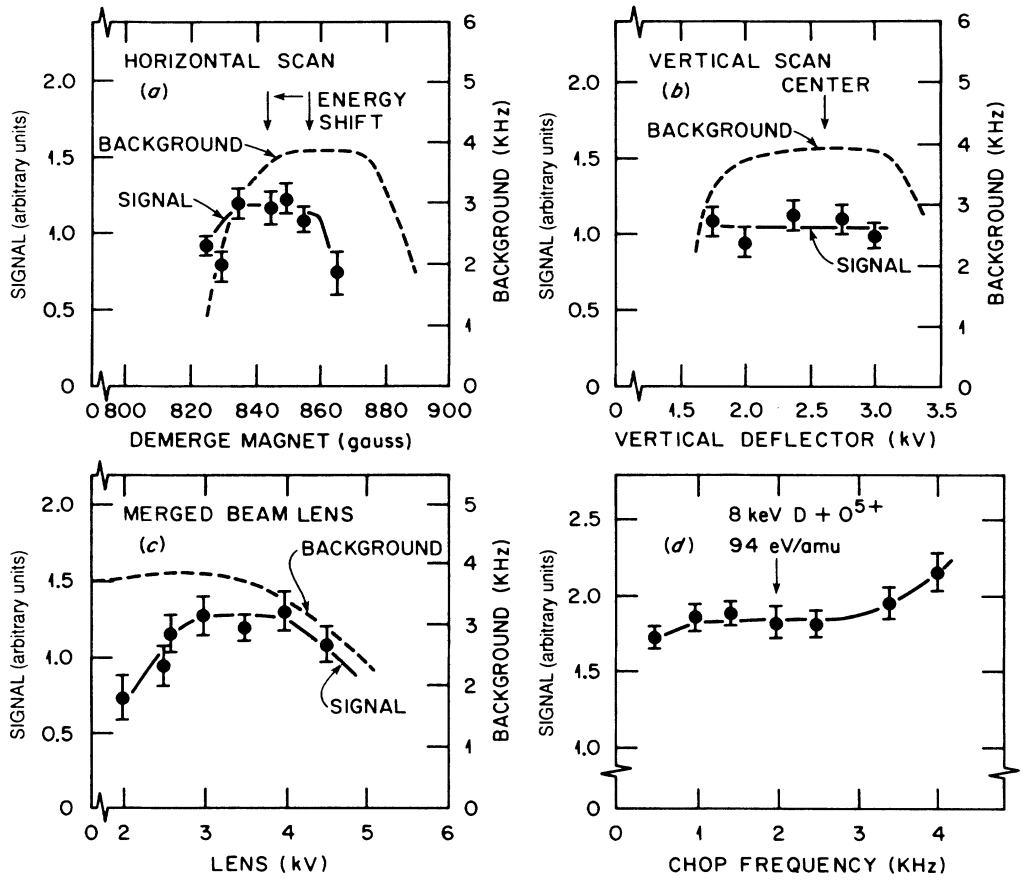

FIG. 11. Various diagnostics performed on the beam-beam signal. (a) Horizontal, (b) vertical, and (c) merge-path Einzel-lens scans are shown for a 6-keV H beam with $E_{rel}=25$ eV/amu. (d) Signal versus chopping frequency for an 8-keV D beam with $E_{rel}=94$ eV/amu. The arrow indicates the typical chopping frequency used during measurements.

switched on and off. To circumvent this problem the large CEM was installed in place of the smaller 1-cm detector. In addition, measurements at low interaction energies were performed with heavier D beams.

The vertical scan [see Fig. 11(b)] was obtained by measuring the signal as the voltage on one of the vertical deflectors (see Fig. 6) was changed. The plateau on the background and signal is at least 900 V wide. This corresponds to a little over 1 keV in H^+ energy. Due to this low-energy dispersion the vertical scan shows no observable shift in energy relative to the background. Vertically, then, the beam-beam products and background can easily be collected simultaneously on the CEM.

The measured signal is also shown [see Fig. 11(c)] as a function of the voltage applied to the Einzel lens in the merged section. A broad plateau is observed indicating sufficient angular collection at this E_{rel} for a 6-keV D neutral beam. There appears to be a slight shift toward higher voltages (stronger focus) for the signal when compared to the background. This is to be expected due to the larger angular scattering of the D^+ produced by electron capture collisions with O^{5+}.

Spurious signals due to spatial beam intermodulation can be both serious and subtle.[25,29] Merged-beams experiments are particularly susceptible to such effects due to the extended interaction length. Local electric fields produced by space charge are also enhanced for multiply charged ion beams. Indeed, space-charge modulation was the most significant single problem to be solved in this experiment. Using the experimental parameters presented in Table I, one can calculate that, in order to determine a signal to an accuracy of 10%, these spurious signals must be eliminated by better than 1 part in 10^3. At lower relative energies elimination of possible spurious signals becomes far more critical, due to the reduced-signal count rate. Figure 11(d) shows the measured signal scanned as a function of the modulation frequency of the two beams. This particular example is for an 8.0-keV D beam at 94 eV/amu. No dependence on frequency was observed except possibly at the very lowest frequency where background pressure modulation by the beams may have an effect on the signal, and the very highest frequencies where spurious effects due to switching the beams on and off may become significant. The sensitivity to background pressure modulation was reduced by collecting the primary beams in the demerging chamber, a

vacuum vessel with limited conductance to the merge section and sufficient pumping to ensure negligible gas loading in the merge section. The beams were switched at frequencies determined to be large enough that the background pressure could not track the ion beams.

Another source of spurious signal due to the chopping of the multicharged ion beam was photons produced in the Faraday cup. Production of these photons continued after the ion beam was turned off, and in fact enough photons were present after the 22-μsec delay built into the chopping scheme to cause false signals. Only after double dispersion of the H^+ products and gold blacking of possible reflecting surfaces could the photons reaching the CEM be reduced to an acceptable level. The fact that the signal remained constant over a wide range of chop frequencies and maintained plateaus in horizontal, vertical, and Einzel scans indicates that the products were being properly collected and discriminated against the background. No systematic dependence on primary beam intensities or measured overlaps was found.

Figure 12 shows the cross-section data taken under different laboratory conditions. In Fig. 12(a) all data are combined and a line is drawn to illustrate the trend of the data. This same line is shown in Figs. 12(b)–12(d), thereby emphasizing any differences due to different laboratory conditions. Included are measurements with 6-keV H, H faster than O^{5+}; 6-keV D, D faster and slower; 8-keV D, D faster and slower; and 9-keV D, D faster and slower. The only significant difference appears in the 6-keV H and D case at ~ 10 eV/amu where the data differ by 10–15 %. This could be due to the reduced angular collection when using the H and D 6-keV beams (see below). After observing this difference the bulk of the data at lower energies was taken with an 8- or 9-keV D beam to ensure the largest angular collection possible. The difference in the 6-keV data was not considered large enough to exclude them from the final tabulation of the cross sections.

B. Uncertainties

The measurements presented here are each independently absolute and involve ground-state reactant beams. The contribution to the reported cross section due to the small fraction of excited states in the neutral beam (estimated in Sec. III to be $\sim 0.01\%$) was measured to be less than 3%. Also, for the collision system and energy range under study, electron capture is dominant over impact ionization in producing H^+ or D^+ products by three orders of magnitude or more.[1] The uncertainty in the energy E_{rel} at which the measurements were taken is shown in Table III. One source of uncertainty is the beam intersection angle of $\approx 0.5°$. This introduces a finite shift in relative energy of ≈ 0.15 eV/amu, and a total spread in energy of 0.30 eV/amu. Since the shift is always toward higher energies, 0.15 eV/amu was added to each energy. Another source of uncertainty in E_{rel} is the uncertainty in the primary-beam laboratory energies. As discussed in Sec. II, these uncertainties are deamplified when transformed to the center-of-mass frame, and the

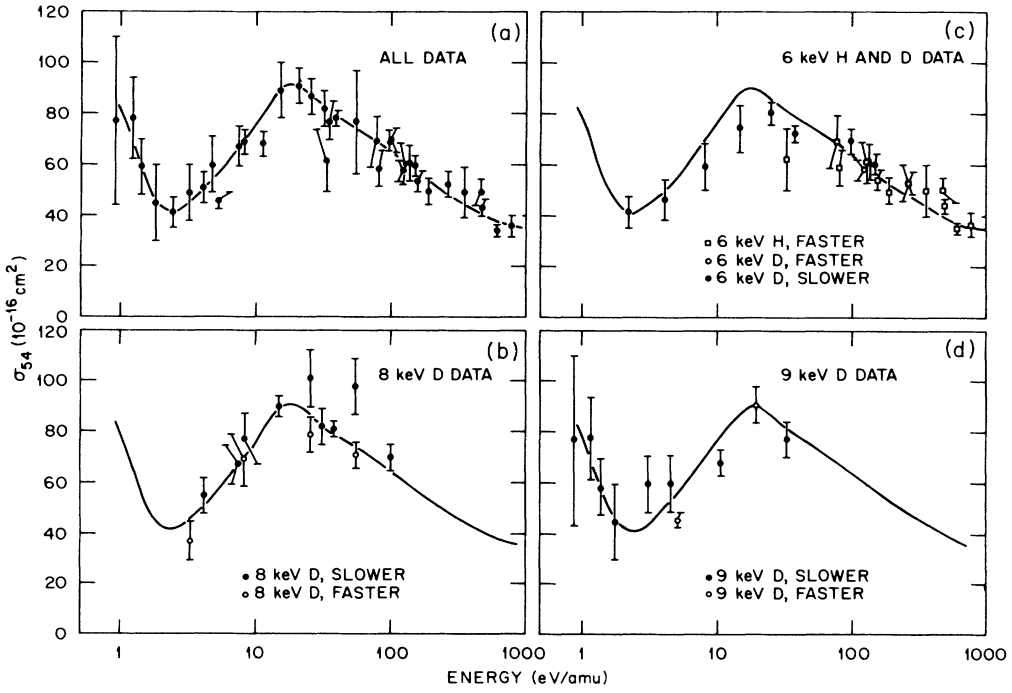

FG. 12. Data taken under different laboratory conditions. (a) All data, under all conditions, are plotted and a line is drawn to guide the eye through the scatter in the data points. The data taken with (b) 6-keV H and D, (c) 8-keV D, and (d) 9-keV D beams are compared with the line from (a) representing the average of all the data.

TABLE III. Uncertainties in the relative collision energy E_{rel} due to uncertainties in the intersection angle and energies of the primary beams. The numbers presented in this table have units of eV/amu.

E_{rel}	ΔE_θ ($\Delta\theta = 0.5°$)	$\Delta E_{O^{5+}}$ ($\Delta E = 100$ eV)	$\Delta E_{H\text{ or }D}$ ($\Delta E = 10$ eV)	ΔE_{total}
1	0.3	0.1	0.1	0.3
10	0.3	0.3	0.25	0.5
100	0.3	0.9	0.9	1.3
1000	0.3	3.2	3.2	4.5

resulting values are given in Table III. Adding all the uncertainties in quadrature gives an estimate of the uncertainty at the several different energies shown.

Uncertainties in the cross-section values are presented in Table IV. All uncertainties are evaluated at a level consistent with the 90% confidence reported for the statistical reproducibility in the measurements. Adding in quadrature gives an estimate for the total systematic uncertainty. Adding the statistical and systematic uncertainties in quadrature results in an estimate for the total absolute uncertainty and is presented with the data in Sec. V.

Another potential source of error in all such low-energy measurements is the finite angular collection of the apparatus. Even with the advantage of the large angular compression inherent in the merged-beams technique, angular scattering in the laboratory frame may exceed angular collection. Figure 13 shows the estimated angular collection of the apparatus for measurements performed with a 6-keV H and a 9-keV D beam (see Fig. 4) plotted with a crude estimate for the angular scattering.[14] This model uses Rutherford scattering formulas assuming zero interaction in the approach of the ion to the neutral and Coulomb scattering for the products after the collision. It may be seen that for the measurements performed with the 6-keV neutral H beam, the angular collection is not sufficient in terms of this estimate for the angular scattering. However, for the 9-keV D case, the angular collection of the apparatus appears to be sufficient. Since measurements at low energies were consistent with the results using 9-keV D, any interpretation of the data reported in this paper should consider the finite angular collection of the apparatus to be represented by the collection for 9-keV D as shown in Fig. 4 and tabulated in Table II.

V. RESULTS AND DISCUSSION

The data for the $O^{5+}+H(D)$ system are listed in Table V. The uncertainty in the energy is consistent with a 90% confidence level. Along with each measurement, the statistical uncertainty estimated at two standard deviations (90% confidence level) and the total absolute uncertainty are listed. The absolute uncertainty is also con-

TABLE IV. Systematic uncertainties in σ estimated at a 90% confidence level (CL).

Beam intensity measurements				
O^{5+}			2%	
H (D)			5%	
Product detection H^+ (D^+)				
Particle detection efficiency			2%	
Counting efficiency			2%	
Background subtraction	1 (eV/amu)	10 (eV/amu)	100 (eV/amu)	1000 (eV/amu)
(chop scheme)	3%	1%	0.3%	0.1%
Beam overlap				
Form factor measurement			5%	
Form factor interpolation or extrapolation			6%	
Effective interaction length				
Merge length L			1%	
$v_1 v_1 / v_r$ determination	1 (eV/amu)	10 (eV/amu)	100 (eV/amu)	1000 (eV/amu)
	8%	1.5%	0.4%	0.1%
H (D) excited-state contribution			3%	
Quadrature sum	1	10	100	1000
	13%	11%	10%	10%

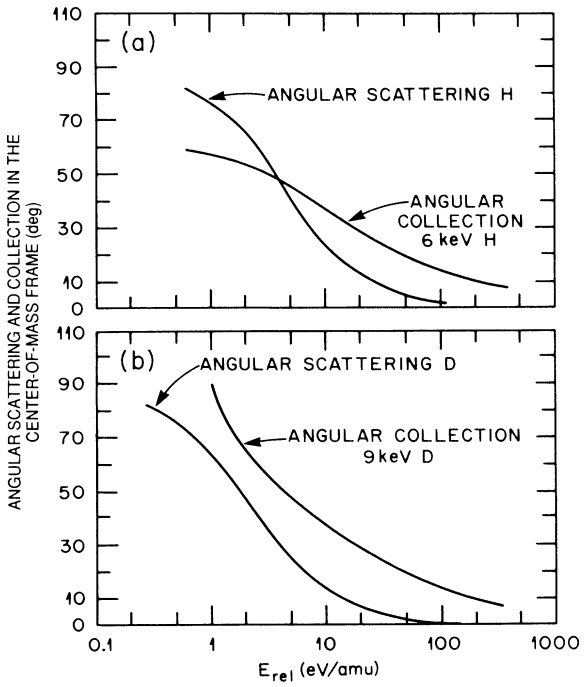

FIG. 13. Angular scattering and collection in the center-of-mass frame are compared for measurements performed with (a) 6-keV H beam, and (b) 9-keV D beam.

sistent with a 90% confidence level and was determined by summing the statistical uncertainty and estimated systematic uncertainties in quadrature.

The independently absolute cross sections for the $O^{5+}+H(D)$ system are plotted in Fig. 14 as a function of the relative energy. Also shown are the various theoretical calculations and other experimental results. As may be seen from the figure, there is good agreement with the previous measurements of Phaneuf *et al.*[12] which extend down to 80 eV/amu. These low-energy measurements were performed using a laser ion source with a hydrogen oven as a target. The density of atomic hydrogen in the oven was determined by a relative calibration. There are also two unpublished data points by Meyer *et al.*[31] which were measured with the ORNL-ECR ion source and the same hydrogen oven. Also shown are the full quantal theoretical calculations of Bottcher and Heil[32] which include capture to the $n=4$ molecular Σ and Π states for the $O^{4+}+H^{+}$ system. All show good agreement in this energy range ($E_{rel}>10$ eV/amu).

As may be seen in Fig. 14, the cross section unexpectedly decreased when the measurements were extended below 10 eV/amu. This decrease is in contradiction to the energy behavior shown in the full quantal calculations of Gargaud and McCarroll[23] who predict an increase in σ_{54} as E_{rel} decreases. At first this observed decrease was thought to be due to a loss of collected signal as a result of large angular scattering of the products. Although the angular collection of the apparatus is less than 90° in this energy range, the following reasons suggest that the angular collection is sufficient: (1) data taken with 6-keV H and D, 8-keV D, and 9-keV D neutral beams are consistent with each other even though the angular collection, especially at low energies, is quite different; (2) the angular collection obtained with the 9-keV D neutral beam is significantly larger than the crude estimate predicted by Rutherford-type scattering (see Fig. 13); (3) The angular collection of the apparatus could also be varied by varying the voltage applied to the merged-path Einzel lens. Where signal-to-noise-ratio levels permitted, these scans showed sufficient plateaus with no observation of a sharp focus. Indeed, inspection of the energy dependence of Gargaud and McCarroll's $4s$ and $4p$ partial-cross-section calculation[23] shows that the experimental energy dependence can be somewhat better accounted for by different weighting in the $n=4$ shell, although no such weighting can reproduce the measured energy dependence below 20 eV/amu.

For measurements below 2 eV/amu the sharp increase observed in σ_{54} is suggestive of the $1/v$ dependence predicted by the classical orbiting model.[9,11] According to this model, as the ion and neutral atom approach, a dipole is induced in the neutral atom, causing an attractive force and possible orbiting trajectories. The interaction potential is given by

$$V(r)=\frac{-q^2\alpha}{2r^4}\ , \tag{11}$$

where α is the polarizability of the neutral atom, q is the charge of the ion, and r is the internuclear separation. For each collision velocity there exists a critical impact parameter b_0, such that for $b>b_0$ the ion and neutral atom come no closer than $b_0/\sqrt{2}$ and for $b<b_0$ the ion and neutral atom follow a collapsing orbit which finally crosses into a reaction sphere. Assuming that for internuclear separations greater than the radius of the reaction sphere no reaction takes place and for separations less than this radius a reaction is guaranteed, the cross section is given by

$$\sigma(v)=\pi b_0^2=\frac{\pi}{v}\left[\frac{4q^2\alpha}{\mu}\right]^{1/2}\ , \tag{12}$$

where all quantities are in atomic units. For the $O^{5+}+D$ system, $\alpha(D)=\frac{9}{2}$ a.u., and at 1 eV/amu, the critical impact parameter $b_0=7.6$ a.u. The resultant cross section for this model is shown in Fig. 14, and can be seen to closely approximate the measured energy dependence below ≈ 2 eV/amu. However, as pointed out by Henchman,[33] it may be inappropriate to arbitrarily apply this simple classical orbiting picture to electron-capture collisions, where the important potential curve crossings often occur at large internuclear separations (i.e., outside the "reaction sphere").

In any case, the trajectories of the reactants are certainly influenced by the weak ion–induced-dipole attraction at very low collision energies (typically below 1 eV/amu). This attractive force allows collisions with larger impact parameters to sample smaller internuclear

TABLE V. Experimental electron-capture cross sections for $O^{2+}+H(D)\rightarrow H^{+}(D^{+})$.

E_{rel} (eV/amu)	ΔE_{rel} (eV/amu)	σ_{54} (10^{-16} cm^2)	Relative uncertainty (90% CL) (10^{-16} cm^2)	Total absolute uncertainty (10^{-16} cm^2)
0.9	0.3	77	33	34
1.2	0.3	78	16	18
1.4	0.3	59	11	14
1.8	0.3	45	15	16
2.4	0.3	41	6	8
3.2	0.3	45	11	12
4.1	0.4	51	6	8
4.7	0.4	60	11	14
5.2	0.4	46	3	7
7.3	0.4	67	8	11
8.2	0.5	68	5	10
11.1	0.5	68	5	9
14.8	0.6	87	11	14
20.4	0.7	91	7	12
25.1	0.7	82	7	12
31.0	0.8	82	7	11
32.8	0.8	62	12	14
33.8	0.8	77	7	10
37.6	0.9	78	3	9
54.1	1.0	76	11	14
76.8	1.2	69	10	12
80.1	1.2	59	7	9
97.0	1.3	69	5	9
98.8	1.3	70	5	9
121	1.5	58	4	8
129	1.5	61	8	10
135	1.6	61	7	10
149	1.6	60	4	7
154	1.7	54	4	7
188	1.8	50	5	7
261	2.2	53	5	7
353	2.5	50	10	11
457	2.9	50	5	7
474	3.0	44	3	6
595	3.3	35	2	4
766	3.8	37	4	6

distances than would otherwise be possible. To produce an enhancement in the electron-capture cross section, a potential curve crossing which can lead to capture must exist at relatively small internuclear separations. Thus, as the collision velocity decreases, trajectories with progressively larger impact parameters sample this inner crossing, producing an enhancement in the capture cross section which varies inversely with velocity. Watson and Christensen[34] have included such trajectory effects in Landau-Zener and full quantal calculations of electron capture for the $N^{3+}+H$ system, finding significant enhancement in the cross section only at energies less than 0.1 eV/amu. For the same system but for energies <20 meV, a partial-wave scattering calculation by Rittby *et al.*[35] shows the presence of a rich resonance structure interpreted in terms of quasibound states associated with classical orbiting (the maximum trajectory effect). The $O^{5+}+H(D)$ collision system may be a better candidate for uncovering such effects experimentally, since the attraction is enhanced for larger ionic charges, and thus trajectories will begin to be affected at higher velocities.

The ion–induced-dipole attraction is taken into account in the molecular perturbed-stationary-state calculations of Gargaud and McCarroll, which disagree with experiment for $O^{5+}+H$ at the lowest energies. The dominant $O^{4+}(1s^2 2s 4l)+H^{+}$ product states all have curve crossings with the incident channel at internuclear separations in the range 10–14 a.u. Corresponding crossings leading to $O^{4+}(1s^2 2s 3l)$ products occur in the range 3–4 a.u., and are predicted to contribute negligibly to the total capture cross section over the energy range of the calculations. However, Gargaud[23(a)] does suggest the possi-

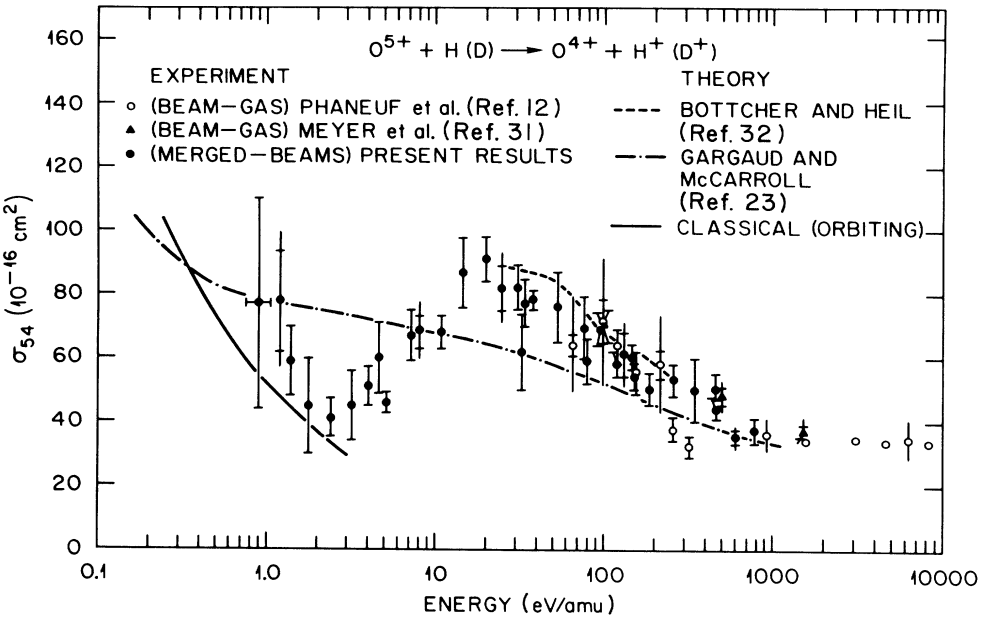

FIG. 14. Comparison of merged-beams data for electron capture in $O^{5+}+H$ collisions with previous measurements and theory. The present data are presented with inner and outer bars denoting relative and estimated total experimental uncertainties, as listed in Table V. The energy uncertainty is denoted by a horizontal bar at the lowest energy where the uncertainty is relatively the largest.

ble significance of product channels involving capture plus excitation of the ion core, such as $O^{4+}(1s^2 2p\,3l)+H^+$, for which calculations have not yet been initiated. These channels cross the incident channel at internuclear separations in the range 6–10 a.u.

The importance of such two-electron processes for our collision system has been estimated by Meyer.[36] In an independent electron model, transition matrix elements for this capture-excitation process may be expressed as the product of a dipole matrix element for $2s$-$2p$ excitation, and a matrix element for single capture. Estimates of such matrix elements[37,38] suggest that they are not negligibly small for the $O^{5+}+H$ system. In fact, Landau-Zener calculations performed by Meyer[36] show that for these states there is an enhancement below 1 eV/amu which is directly attributed to the ion-induced-dipole attraction. However, when the dominant crossings ($O^{4+}1s^2 2s4l$) which occur at larger internuclear separations are considered, it is unclear how the crossings for capture plus excitation could be accessed. It may, nevertheless, be important to include these states in a more comprehensive coupled-channel calculation.

ACKNOWLEDGMENTS

This research was sponsored by the Division of Chemical Sciences, U. S. Department of Energy, under Contract No. DE-AC05-84OR21400 with Martin Marietta Energy Systems, Inc. This research would not have been possible without the stable, high-intensity beams of multiply charged ions produced by the ORNL-ECR ion source. The authors are grateful to F. W. Meyer for developing the ORNL-ECR source, and to technologist J. W. Hale for maintenance of laboratory equipment. We are indebted to C. F. Barnett, C. Bottcher, and D. H. Crandall for many fruitful discussions, and in particular to F. W. Meyer and R. K. Janev for performing calculations which helped to clarify the mechanisms for electron capture at low energies. Special thanks are due to M. Gargaud, R. McCarroll, C. Bottcher, and T. G. Heil for communicating their theoretical results prior to publication. M. S. H. was supported by the Postgraduate Research Training Program, administered by Oak Ridge Associated Universities (ORAU) for the U. S. Department of Energy. P. A. S. was supported by the ORAU Summer Faculty Research Participation Program.

*Permanent address: Lincoln Laboratory, Massachusetts Institute of Technology, Lexington, MA 02137-0073.

[1]R. K. Janev, L. P. Presnyakov, and V. P. Shevelko, *Physics of Highly Charged Ions* (Springer-Verlag, Berlin, 1985).

[2]H. B. Gilbody, Adv. At. Mol. Phys. **22**, 143 (1986).

[3]F. W. Meyer, A. M. Howald, C. C. Havener, and R. A. Phaneuf, Phys. Rev. A **32**, 3310 (1985).

[4]E. H. Nielsen, L. H. Anderson, A. Bárány, H. Cederquist, P. Hvelplund, H. Knudsen, K. B. MacAdams, and J. Sorensen, J. Phys. B **17**, L139 (1984).

[5]D. Dijkkamp, D. Ćirić, and F. J. de Heer, Phys. Rev. Lett. **54**, 1004 (1985).

[6]W. Fritsch and C. D. Lin, J. Phys. B **17**, 3271 (1984).

[7]T. A. Green, E. J. Shipsey, and J. C. Browne, Phys. Rev. A **25**,

1364 (1982).
[8]C. Bottcher and T. G. Heil, Chem. Phys. Lett. **86**, 506 (1982).
[9]R. E. Olson, *Electronic and Atomic Collisions*, edited by N. Olda and K. Takayanagi (North-Holland, Amsterdam, 1980), p. 391.
[10]R. McCarroll and P. Valiron, Astron. Astrophys. **78**, 177 (1979).
[11]G. Gioumousis and D. P. Stevenson, J. Chem. Phys. **29**, 294 (1958).
[12]R. A. Phaneuf, I. Alvarez, F. W. Meyer, and D. H. Crandall, Phys. Rev. A **26**, 1892 (1982).
[13]R. D. Rundel, D. E. Nitz, K. A. Smith, M. W. Geis, and R. F. Stebbings, Phys. Rev. A **19**, 33 (1979), and references therein.
[14]R. E. Olson and M. Kimura, J. Phys. B **15**, 4231 (1982).
[15]J. R. Peterson, W. H. Aberth, J. T. Moseley, and J. R. Sheridan, Phys. Rev. A **3**, 1651 (1971).
[16]J. Weiner, W. B. Peatman, and R. S. Berry, Phys. Rev. A **4**, 1824 (1971).
[17]P. K. Rol, E. A. Entemann, and K. L. Wendell, J. Chem. Phys. **61**, 2050 (1974).
[18]S. M. Trujillo, R. H. Neynaber, and E. W. Rothe, Rev. Sci. Instrum. **37**, 1655 (1966).
[19]P. M. Koch and J. E. Bayfield, Phys. Rev. Lett. **34**, 448 (1975).
[20]W. R. Gentry, D. J. McClure, and C. H. Douglass, Rev. Sci. Instrum. **46**, 367 (1975).
[21]M. Burniaux, F. Brouillard, A. Jognaux, T. R. Grovers, and S. Szucs, J. Phys. B **10**, 24221 (1977).
[22]R. H. Neynaber and G. D. Magnuson, J. Chem. Phys. **61**, 749 (1974).
[23](a) M. Gargaud, thesis, L'Université de Bordeaux I, 1987; (b) M. Gargaud and R. McCarroll (unpublished).
[24]K. L. Wendell and P. K. Rol, J. Chem. Phys. **61**, 2059 (1974).
[25]P. O. Taylor, R. A. Phaneuf, and G. H. Dunn, Phys. Rev. A **22**, 435 (1980).
[26]B. Van Zyl, N. G. Utterback, and R. C. Amme, Rev. Sci. Instrum. **47**, 814 (1976).
[27]H. J. Kim and F. W. Meyer, Phys. Rev. A **26**, 1310 (1982).
[28]F. W. Meyer, Nucl. Instrum. Methods B **9**, 532 (1985).
[29]K. T. Dolder, *Physics of Ion-Ion and Electron-Ion Collisions*, edited by F. Brouillard and J. W. McGowan (Plenum, New York, 1983), p. 373.
[30]W. B. Herrmannsfeldt, electron trajectory program, SLAC-226, Stanford University, 1979.
[31]F. W. Meyer, A. M. Howald, C. C. Havener, and R. A. Phaneuf (unpublished).
[32]C. Bottcher and T. G. Heil (unpublished); for general method, see Ref. 8.
[33]M. Henchman, in *Ion-Molecular Reactions*, edited by J. L. Franklin (Plenum, New York, 1972), Vol. 1, pp. 101–259.
[34]W. D. Watson and R. B. Christensen, Astrophys. J **231**, 627 (1979).
[35]M. Rittby, N. Elander, E. Brändas, and A. Bárány, J. Phys. B **17**, L677 (1984).
[36]F. W. Meyer (private communication).
[37]R. K. Janev (private communication).
[38]S. E. Butler and A. Dalgarno, Astrophys. J. **241**, 838 (1980).